Lagrangian Delay Predictive Model for Sector-Based Air Traffic Flow

Alexandre M. Bayen*
University of California at Berkeley, Berkeley, California 94720-1710
Pascal Grieder†
Swiss Federal Institute of Technology, CH-8092 Zurich, Switzerland
George Meyer‡
NASA Ames Research Center, Moffett Field, California 94035-1000
and
Claire J. Tomlin§
Stanford University, Stanford, California 94305-4035

A control theoretical model of sector-based air traffic flow is derived using hybrid automata theory. This model is Lagrangian, because it models the properties of the system along its trajectories. A subset of this model is used to generate analytic predictions of air traffic congestion: A dynamic sector capacity is defined and derived that is used for predicting the time it takes to overload a given portion of airspace. This result links the Lagrangian approach with Eulerian models, which account for temporal variations of parameters in a fixed volume. To determine the accuracy of predictions, an air traffic flow simulator is designed and validated. The simulator is then used to show that flow scheduling and conflict resolution may be decorrelated by reducing aircraft density.

Nomenclature

$\boldsymbol{a}$	=	vector $[a_1^0, \ldots, a_N^0]$ of initial arc length distances for N aircraft
a_i^0	=	initial arc length distance of aircraft i from San Francisco Airport along arrival route
$\boldsymbol{b}$	=	vector $[b_1, \ldots, b_N]$ for N aircraft used for computing individual b_i
b_i	=	variable used to compute mode switching time of aircraft i
d_{LOS}	=	distance at which a loss of separation (LOS) occurs
$d_{\min}^i$	=	minimum distance from aircraft i to any other aircraft in sector
$f()$	=	penalty function for aircraft separation (associated to $d_{\min}^i$ for all i)
J	=	cost function encoding air traffic control (ATC) controller action and sector state
$J_{\{\text{given action}\}^i}$	=	cost associated to {given action} of controller (vector for spacing, shortcut, etc.) for aircraft i
M	=	Mach number
N	=	total number of aircraft in sector of interest at given time, $N = N(t)$
N_{choice}	=	number of aircraft selected for analysis by simulator
N_{limit}	=	dynamic capacity of sector of interest
N_{moved}	=	total number of aircraft moved at simulator iteration
n_{LOS}^i	=	number of LOS for aircraft i that would happen with given set of maneuvers
n_{maneuver}	=	number of maneuvers simulator can assign to aircraft at any given time
$\mathbb{R}$	=	set of real numbers
R_ψ	=	rotation matrix of angle ψ for heading changes
T_{breach}^i	=	boundary condition breach time of aircraft i
T_{limit}	=	saturation time of sector of interest
$\text{TOA}_{\text{pred}}^i$	=	predicted time of arrival (TOA) of aircraft i [at terminal radar approach control (TRACON)]
$\text{TOA}_{\text{real}}^i$	=	actual TOA of aircraft i (at TRACON)
t_{block}	=	time at which metering condition is imposed
t_i^{switch}	=	time at which aircraft i undergoes mode switch by air traffic control (ATC)
$\boldsymbol{v}_{\text{current heading}}$	=	velocity vector of given aircraft at its current heading
$v_{\max}$	=	maximum aircraft speed
$v_{\min}$	=	minimum aircraft speed
v_{nom}	=	nominal aircraft speed
$w_{\text{given action}}$	=	weight (penalty) associated to given action of controller
x	=	distance to destination airport along flight plan
x_{ex}	=	distance from airport at which metering is applied
$\boldsymbol{x}_i$	=	position of aircraft i
x_i^{switch}	=	location at which aircraft i undergoes mode switch by ATC
ΔL	=	requested outflow separation for merging traffic in region of interest
ΔL_{in}	=	imposed inflow separation for cross traffic in region of interest
ΔL_{out}	=	requested outflow separation for cross traffic in region of interest
ΔT_{act}	=	time period for one iteration of simulator
ΔT_{LOS}^i	=	time until next predicted occurrence of loss of separation for aircraft i
ΔT_{out}	=	outflow period of region of interest (one aircraft every ΔT_{out} time units)

*Assistant Professor, Department of Civil and Environmental Engineering, 711 Davis Hall; bayen@ce.berkeley.edu. Member AIAA.

†Nachdiplomstudium in Betriebswissenschaften Student; currently Associate, McKinsey and Co., Alpenstrasse 3, 8065 Zurich, Switzerland; pascal_grieder@mckinsey.com.

‡Research Scientist, Mail Stop 210-10; gmeyer@mail.arc.nasa.gov.

§Associate Professor, MC 4035, Department of Aeronautics and Astronautics and Courtesy Associate Professor, Department of Electrical Engineering, 028A Durand Building; tomlin@stanford.edu. Member AIAA.

Introduction

THE National Airspace System (NAS) is a large-scale, hierarchical, nonlinear dynamic system. At the top of the control hierarchy, a single Air Traffic Control System Command Center (ATCSCC) in Herndon, Virginia, supervises the overall traffic flow (Fig. 1). This is supported by 22 (20 in the continental United States) Air Route Traffic Control Centers [(ARTCCs) or simply, Centers] at the lower control layer, organized by geographical region up to 60,000 ft (Refs. 1–6). Each Center is subdivided into 20–80 sectors, with at least one air traffic controller responsible for each sector. The maximum number of aircraft that can be in a sector is a function of the sector geometry and the procedures used for controlling traffic. Typical values are between 10 and 20 aircraft. The air traffic controller is responsible for preventing losses of separation (LOS) between aircraft, keeping them separated by more than 5 n mile horizontally; 1000 ft vertically below 29,000 ft; and 2000 ft vertically above 29,000 ft. For aircraft flying under instrument flight rules, the air traffic controller has access to the aircraft's flight plan and may revise the altitude; provide temporary heading assignments; and amend the route, speed, or profile to attempt to maintain efficiency and to keep aircraft separated. The current control structure is presented in Fig. 1.

Existing NAS modeling tools span the modeling of runway and airport capacity and terminal operations, through airspace operations and conflict resolution,[7,8] to human factors and man–machine integration. References 9 and 10 are surveys of NAS modeling and conflict detection and resolution methods. A recent tool, Future ATM (Air Traffic Management) Concepts Evaluation Tool (FACET),[11,12] provides a NAS simulation tool from a traffic flow management (TFM) point of view. FACET can also be used for playing back recorded enhanced traffic management system (ETMS) data. [Data are collected from the entire population of flights with filed flight plans in the NAS. ETMS data are sent from the Volpe National Transportation System Center to registered participants via the aircraft situation display to the industry electronic file server. A file containing all recorded data is generated. It displays for each aircraft the current flight data (time, position), as well as the filed flight plan (in terms of navigation aids, airways, fixes, etc.). The update rate of the measurements is of the order of 1 min.] The goal of the present research is to develop a model that complements existing tools by providing a control theoretic component for modeling the influence of air traffic control (ATC). Whereas the additional logic required to model the actions of the air traffic controller does not pose a significant computational problem if the aircraft density in the airspace is low, it becomes an issue as the density increases. (The growth of computational cost is exponential with aircraft number per sector.) The long-term goal of increasing capacity, as well as safety, in the NAS cannot be achieved without an in-depth analysis of the applied control logic and modeling the current airspace with sufficient accuracy. Such a model would improve ATC delay prediction and, thus, enable a wide array of applications.

In this paper, a model, as well as analytic and simulation results, of the aircraft and controller actions within a sector of airspace are presented. The Lagrangian approach is based on the trajectories of the aircraft and trajectory dependent aggregate quantities such as the average number of aircraft in a portion of airspace, as well as their momentum and speed.

Although several NAS models in the literature are trajectory based,[11,13–18] they are explicitly related to an Eulerian framework. The Lagrangian model developed in this paper is linked with Eulerian models.[19,20] Eulerian approaches are control volume based. Thus, they account for temporal fluctuations of quantities in a given volume, for example, the number of aircraft in a sector as a function of time. The connection between these two approaches is made through the concept of sector dynamic capacity that is introduced in this paper and that is related to flow rate constraints[14] and complexity metrics.[21] The Lagrangian model presented here can be used to study the effect of aircraft flow density requirements at sector boundaries, due to, for example, miles-in-trail requirements at airports. (The terminology n miles in trail is a standard term used by ATC. It means that aircraft follow each other separated by n miles.) This model makes it possible to predict how the current system might react to imposed flow conditions. Given a set of flight plans, the model enables evaluation of the effectiveness of different controller policies in minimizing delays.

This paper has two components: 1) airspace modeling and analysis and 2) validation and simulation. In the first part, a hybrid-system-based model for a controlled sector is presented. Hybrid means that the model allows for continuous and discrete behavior at the same time; it will be defined more precisely later. The hybrid system model for each aircraft encodes simple aircraft dynamics under the discrete action of the air traffic controller. The number of such actions is large but finite and consists of simple instructions such as turn to heading of 30 deg, hold current heading, fly direct to Coaldale (OAL) vhf omni-directional range (VOR), and increase speed to 450 kn. This model is analyzed and used to define the concept of sector dynamic capacity. This concept facilitates the prediction of the time it takes to overload, that is, to reach the maximum authorized number of aircraft in that sector, given sectors of airspace, and thus makes delay predictions possible. If air traffic controllers are assumed to use a subset of their available control actions, the delay prediction results are then related to Eulerian approaches. In the second part of this paper, the earlier results are validated against real data. Because the results cannot be tested on the real ATC system directly, a simulator of the system is designed and implemented in C++ interfaced with MATLAB®. This simulator consists of the mathematical model derived in the first part of the paper, augmented with a logic for switching between the different controller states. This model attempts to reproduce the actions of a human air traffic controller by minimizing cost functions defined over sectors. This simulator was validated by comparing the simulated data against ETMS data. It is shown that the analytical predictions for sector capacity are effectively observed in simulations. Finally, the simulator is used to identify flow conditions under which conflict resolution decorrelates from metering problems, that is, scheduled time of arrival. This result has implications for numerous ATC flow management techniques that rely implicitly on this assumption.[14,19,22,23]

The data presented in this paper pertain to several sectors within the Oakland Center, located in Fremont, California. The methodology, however, is general and would apply to any other en route portion of the NAS. Jeppesen[24] high-altitude en route charts were used for modeling the Oakland Center airspace. The controller model and cost function have been designed based on several hours
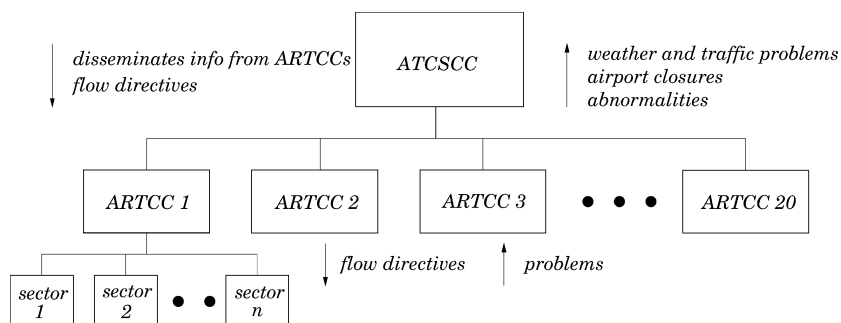

Fig. 1   Control hierarchy in current structure of NAS.

of observations of sector controllers for given sectors at the Oakland Center. The approximations that have been made for the study in this paper are noted throughout. Whereas the model is general, most of the scenarios considered do not represent normal traffic flow. This is because of the interest in modeling delay propagation of the system under stress. Hence, the traffic scenarios modeled represent heavy traffic flow along airways.

The contributions of this paper are a new mathematical model for airspace sectors, based on hybrid system theory; an analytical solution to the Lagrangian problem of delay propagation in the network of airways and its link with Eulerian approaches; and the concept and use of sector dynamic capacity. From the application point of view, the novelty lies in the validation of a control theoretic model of the human air traffic controller and in the validation of the analytical predictions against real data. Finally, the decorrelation results shown by the simulations are new.

This paper is organized as follows: In the next section, the model used for aircraft dynamics and air traffic controller actuation are presented. This model is used to predict the propagation of airspace congestion and to define sector capacity. In the following section, the design of the simulator, its use in validating the analytical predictions, and its use in demonstrating the decorrelation between conflict resolution and flow metering are presented.

Air Traffic Flow Modeling and Analysis

The structure of the NAS is complex, with a multitude of interacting agents and technologies for aircraft monitoring, flow management, communication, and human-centered automation. For the present work, only the features that are important for delay prediction are modeled. The portion of the Oakland ARTCC modeled contains five sectors. These sectors surround the Bay terminal radar approach control (TRACON), which controls aircraft on their approach into San Francisco, San Jose, and Oakland airports. The Bay TRACON is the final destination of the traffic considered.

A sector is modeled by a portion of airspace containing aircraft under the control of a sector controller (Figs. 2 and 3). Within each sector, navigation infrastructure, consisting of airways, waypoints, and navigation aids, is used to guide the flow in desired patterns. Therefore, the structure of the airspace is modeled and used even if it is observed that more than 40% of the aircraft deviate from their filed flight plan. The model permits aircraft to fly at different altitudes, but not to climb or descend. Altitude changes are not crucial for this analysis, but aircraft acceptance rates at destination airports are. Future models might incorporate altitude changes, though, because they sometimes impact workload, for example, in the presence of cross traffic. The applicability of the current model is, thus, limited to sectors in which most of the traffic is arrival traffic, as in Ref. 14, for example.
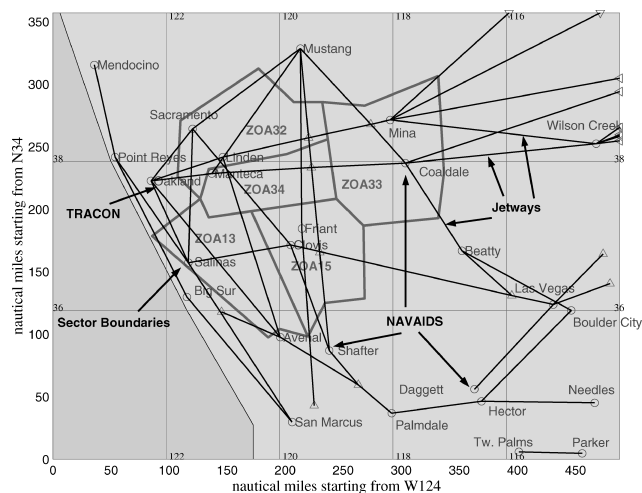

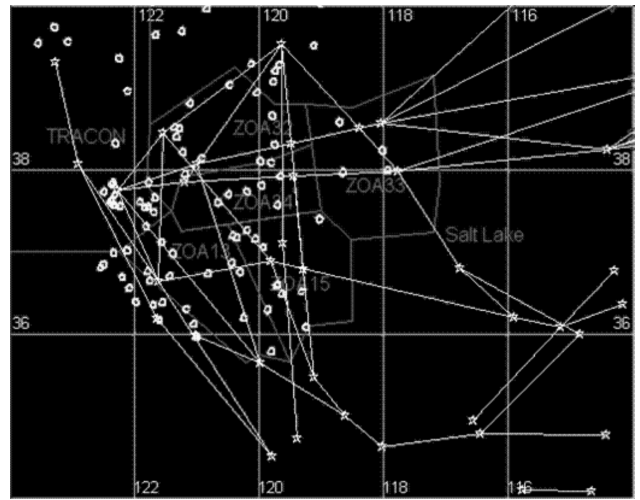Fig. 2 ATC sectors modeled for this study: 32, 33, 34, 13, and 15 within the Oakland ARTCC.

Fig. 3 Visual display of simulator, traffic in Oakland ARTCC.
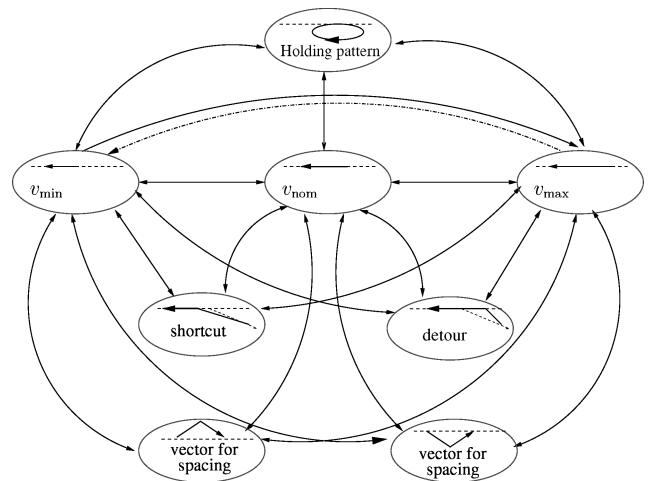

Fig. 4 Hybrid automaton representing action of one controller on single aircraft.

Aircraft Behavior

A hybrid model for each aircraft describes the evolution of a system by a set of discrete modes with associated continuous dynamics and discrete switches, which enable the system to jump from one mode to another instantaneously. The motion of aircraft i is described as

$$\dot{\boldsymbol{x}}_i = \frac{\mathrm{d}\boldsymbol{x}_i}{\mathrm{d}t} = \boldsymbol{v}_i^{\text{current heading}} \tag{1}$$

where $\boldsymbol{v}_i^{\text{current heading}} \in \mathbb{R}^2$ is a constant velocity vector held by the aircraft until the next discrete switch, a heading or speed change that changes $\boldsymbol{v}_i^{\text{current heading}}$. Here, $\boldsymbol{x}_i \in \mathbb{R}^2$ is the planar position of aircraft i. Integration of Eq. (1) over time produces a continuous piecewise affine trajectory. Such a model is preferred over a continuous dynamic model for two reasons. First, the timescale of a change in aircraft behavior, for example, a turn or slow down, is on the order of several seconds, whereas the timescale of a straight line portion of the flight is usually much longer, sometimes 15 min or more; thus, dynamics of such maneuvers are ignored and only their effects are considered (the set of resulting straight lines). Second, the update rate of ATC monitoring is generally not more than 30 s, which makes the details of these maneuvers obscure to the ATC. This approximation is widely accepted in literature.[17,22,25−28]

Observations at the Oakland Center showed that a finite set of maneuvers is used by controllers. Combinations of these maneuvers result in a conflict-free flight environment in which the constraints of the air traffic flow are met. The maneuvers shown in Fig. 4 are realized by changing the speed and the heading of the aircraft [right-hand side of Eq. (1)]. In Fig. 4, each of the eight modes represents

one possible state of the aircraft. The arrows joining these states are the mode switches, initiated by the controller. The validity of models similar to this has been confirmed by statistical studies.[21]

1) For speed change, if ATC employs speed control, the aircraft may decelerate or accelerate without deviating from its flight plan,

$$v_{\text{modified speed}} := \lambda \cdot v_i^{\text{current heading}} \qquad (2)$$

where $\lambda \in \mathbb{R}^+$ defines the magnitude of the velocity change. The model is designed to allow a finite set of speeds, which means that λ has a finite number of acceptable values. This is because aircraft performance is tied to airspeed and because aircraft thrust is limited at altitude. Generally, ATC will not speed up or slow down the aircraft by more than 10% of the current value.

2) The vector-for-spacing (VFS) maneuver consists of a deviation of the aircraft away from its original flight plan for a short time (part 1 of the maneuver) and then a second deviation (recovery maneuver) for bringing it back to its original flight plan (part 2 of the maneuver). This stretches the path that the aircraft must follow and, therefore, results in delay. The maneuver is contained within the extent of the sector. Where R_ψ is the rotation matrix by angle ψ,

$$v_{\text{part1}} := R_\psi \cdot v_i^{\text{current heading}} \quad \text{(first-half of maneuver)}$$

$$v_{\text{part2}} := R_{-2\psi} \cdot v_{\text{part1}} \qquad \text{(second-half of maneuver)} \qquad (3)$$

3) In certain situations, the ATC will have the aircraft "cut" between two airways, a shortcut/detour maneuver that could either shorten or lengthen the flight plan. The decision to command such a maneuver is often dictated by conflict resolution, but could also be used to shorten the overall flight time if sector occupancy allows it (sometimes called "direct-to" by pilots):

$$v_{\text{shortcut}} := R_\psi \cdot v_i^{\text{current heading}} \qquad (4)$$

for the duration of the maneuver, until the next ATC action is taken. Here again, ψ is the heading change angle by which ATC turns the aircraft to achieve the shortcut.

4) Holding patterns are used to hold an aircraft in a given region of airspace before allowing them to follow their original flight plan. This is modeled by assigning the aircraft to a predefined zone and keeping it there while preventing other aircraft from entering that zone.

Lagrangian Analysis of Delay Propagation in NAS

A large proportion of en route and terminal congestion is caused by restrictions imposed at destination airports, due to weather or airport arrival–departure demand. These restrictions are often imposed as miles-in-trail or minutes-in-trail metering constraints, representing the distance (or time) required between aircraft in a flow arriving to the TRACON. Figure 5 shows the topology of the inbound flows
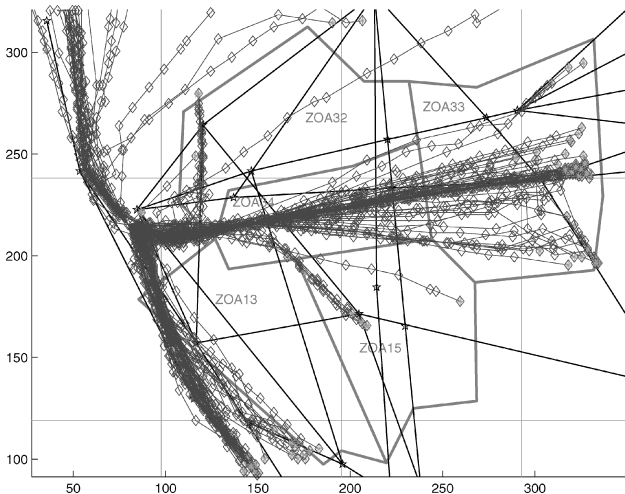
Fig. 5   Overlay of trajectories merging into SFO (11 h of traffic).

into San Francisco Airport (SFO), which are often subject to this type of constraint. These constraints tend to propagate backward from the airport into the airways and result in miles-in-trail constraints imposed at the entry points of each sector. For example, in the case shown in Fig. 5, these metering conditions propagate backward toward the east as follows: TRACON → sector 34 → sector 33 → Salt Lake Center, ...

In the current system, these restrictions are imposed empirically. To ensure maximal throughput into the TRACON, an understanding of 1) how the traffic jams propagate and 2) what the optimal control policy should be under these restrictions is needed. These issues are addressed in the paper.

Shock Wave Propagation

A simple Lagrangian model of merging flows introduced earlier in Refs. 29 and 30 is used for studying the phenomenon of shock wave propagation for metering the merging flows of the type shown in Fig. 5. The concept of dynamic capacity appears naturally in the metering problem, defined as follows.

Given a required spacing of ΔT_{out} between the aircraft (metering constraint), compute a controller policy for routing groups of aircraft to satisfy exactly the metering constraint at the sector exit point while maintaining separation at all times.

The task of meeting metering constraints can be achieved by applying the various control options available to the controller (Fig. 4). Consider a very simple version of the problem, in which the controller uses only two modes (fast and slow). Several methodologies can be used to map the full automaton shown in Fig. 4 to this model: See, for example, Refs. 14 and 23.

To explain the procedure, consider the following example. Let the initial arc length distance of aircraft i be $a_i^0 \in \mathbb{R}$ along its arrival route to the airport. An $a_i^0 = -200$ means that aircraft i has to fly 200 n mile before landing at the destination airport. Let $x_{\text{ex}} \in \mathbb{R}$ be the location at which the metering condition is imposed. For example, $x_{\text{ex}} = -50$ means that the metering is applied 50 n mile from the airport. It is possible to assume without loss of generality that the aircraft are numbered in order of arrival. (The a_i^0 are indexed in increasing order.)

Assume that all aircraft are initially at maximum speed v_{max} and that ATC slows down aircraft i to its minimum speed v_{min} for metering (Fig. 6) at a location x_i^{switch} at time t_i^{switch}, which is unknown for now (Fig. 7). This scenario is represented as a dash–dot line in Fig. 4. The condition that each aircraft cross the metering point x_{ex} at exactly $t_{\text{block}} + (i-1)\Delta T_{\text{out}}$ is imposed, where t_{block} is the time at which the metering condition is initiated. The motion of aircraft under the metering constraint is described by the following kinematic equations:

$$x_i(t) = a_i^0 + v_{\text{max}} t \qquad \text{if} \qquad t \in \left[0, t_i^{\text{switch}}\right] \qquad (5)$$

$$x_i(t) = x_i\left(t_i^{\text{switch}}\right) + v_{\text{min}}\left(t - t_i^{\text{switch}}\right) \qquad \text{if}$$

$$t \in \left[t_i^{\text{switch}}, t_{\text{block}} + (i-1)\Delta T_{\text{out}}\right] \qquad (6)$$

In the preceding formula, the origin of time is taken without loss of generality at $t_0 = 0$. The assumption of continuity of $x_i(t)$ enables
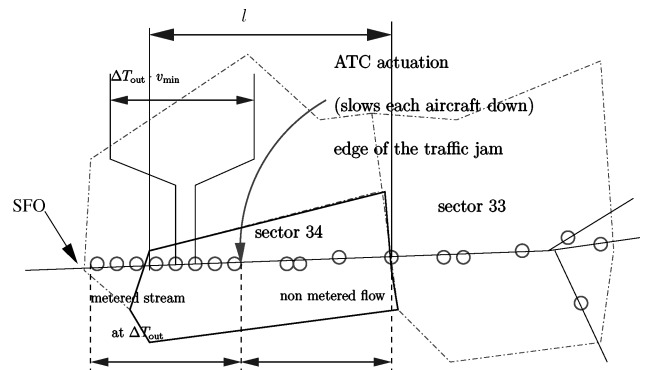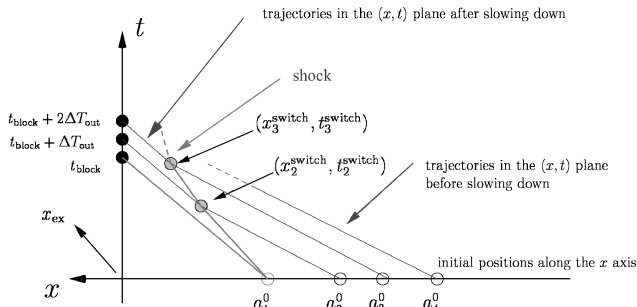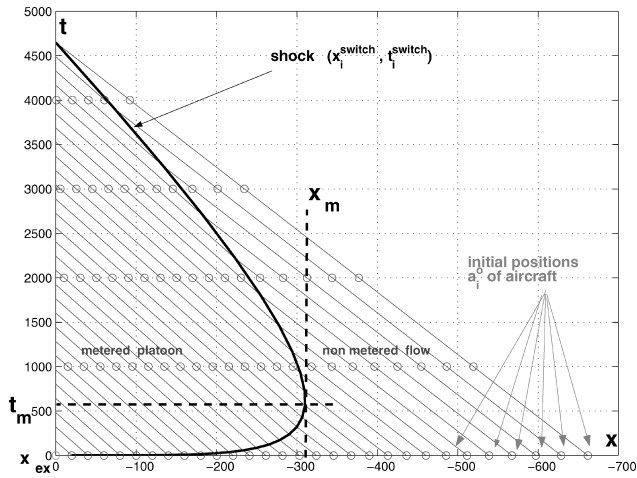
Fig. 6   ATC control for merging flow.

Fig. 7 Shock construction: aircraft trajectories are represented in (x, t) plane.

Fig. 8 Switching curve (shock) for vanishing traffic congestion.

us to solve for t_i^{switch} and $x_i(t_i^{\text{switch}}) := x_i^{\text{switch}}$. The condition for the system (5) and (6) to have a physically acceptable solution is

$$a_i^0 \in [x_{\text{ex}} - v_{\text{max}}(t_{\text{block}} - (i-1)\Delta T_{\text{out}}),$$

$$x_{\text{ex}} - v_{\text{min}}(t_{\text{block}} - (i-1)\Delta T_{\text{out}})] \qquad (7)$$

When Eq. (7) is met, the analytical solution of Eqs. (5) and (6) provides the location of the edge of the congestion front in space and time,

$$t_i^{\text{switch}} = \frac{x_{\text{ex}} - v_{\text{min}}t_{\text{block}} - (i-1)\Delta L - a_i^0}{v_{\text{max}} - v_{\text{min}}}$$

$$x_i^{\text{switch}} = a_i^0 + \frac{v_{\text{max}}\left[x_{\text{ex}} - v_{\text{min}}t_{\text{block}} - (i-1)\Delta L - a_i^0\right]}{v_{\text{max}} - v_{\text{min}}} \qquad (8)$$

where $\Delta L := v_{\text{min}}\Delta T_{\text{out}}$ is the metered spacing at the outflow of the sector. At a given time t, the metered stream consists of the set of aircraft such that $t_i^{\text{switch}} \le t$. These aircraft have already been slowed down (Fig. 6) and congest the airspace they occupy. It follows directly from Eq. (8) that the congested portion of airspace, that is, the stream of aircraft metered at ΔT_{out} in Fig. 6, will not grow in length if the two following conditions are met:

$$t_i^{\text{switch}} < t_{i+1}^{\text{switch}} \Leftrightarrow \Delta L < a_i^0 - a_{i+1}^0$$

$$x_{i+1}^{\text{switch}} < x_i^{\text{switch}} \Leftrightarrow (v_{\text{min}}/\Delta L) < \left[v_{\text{max}}\big/\left(a_i^0 - a_{i+1}^0\right)\right] \qquad (9)$$

Condition (9) is a sufficient condition for traffic congestion to decay, which can be observed by inspection of the slope of the switching curve of points $(x_i^{\text{switch}}, t_i^{\text{switch}})$ displayed in Figs. 7 and 8. The switching curve can also be called a shock wave, which traditionally refers to the moving interface between a medium of high density

and a medium of low density (in the present case, density of aircraft). In Fig. 7, x denotes the distance to the metering point (SFO). The lines are the trajectories of the aircraft in the (x, t) space. The positions of aircraft are represented every 1000 s as dots. Once they have passed through the shock, they are separated by $v_{\text{min}}\Delta T_{\text{out}}$. The point (x_m, t_m) is the farthest reachable point by this traffic congestion. Note that the slope of the lines changes through the shock. The slope difference can hardly be seen visually because the speed change is small.

Equation (9) is a local property of the problem in that it depends only on $a_i^0 - a_{i+1}^0$ and not on all of the aircraft. The second equation in Eq. (9) corresponds, in fact, to a one-dimensional discretized steady Lighthill–Whitham–Richard equation, which appears naturally in highway congestion problems.[31] This result is obtained through a Lagrangian analysis, which links it to Eulerian approaches such as those in Refs. 19 and 20, which are based on conservation equations. It relates local properties of the flow (direction and speed of propagation congestion, aircraft density on an airway) to global quantities (here, the trajectories of the aircraft). This is important because it, thus, enables one to link quantities that are easy to access (flight plans and, thus, trajectories) to density (and, thus, sector counts), which are harder to predict. This result is illustrated in Fig. 7: The aircraft trajectories are represented in the (x, t) plane. They originate at $t = 0$ from the horizontal axis (white circle on each trajectory). After some amount of time, the aircraft may be switched to speed v_{min} at location $(x_i^{\text{switch}}, t_i^{\text{switch}})$ (shaded circle on each trajectory). Ultimately, they reach x_{ex}, the entrance of TRACON (black circle).

The condition that each aircraft reaches x_{ex} exactly at the scheduled time of arrival is restrictive. From the TFM (a set of ARTCC controllers in charge of flow management at the center level) point of view, the actual crossing times are not important, but the flow rate is. Therefore, it is meaningful to pose the problem as follows.

Given $\{a_i^0\}_{i \in [1,N]}$, compute the switching policy that delivers at most one aircraft every ΔT_{out} s at the location x_{ex} while maintaining separation and that minimizes the arrival time of aircraft N.

This problem may be posed as a linear program. 1) Minimize the arrival time of aircraft N while 2) separating the aircraft by more than ΔT_{out} at x_{ex}, with 3) at most one switch between the initial position $a_i^0 \le x_{\text{ex}}$ and the exit x_{ex} of the considered airspace as follows:
1) Minimize

$$[0, \cdots 0, -1]\boldsymbol{b}$$

2) subject to

$$\begin{bmatrix} -1 & 1 & 0 & \cdots & \cdots & 0 \\ 0 & -1 & 1 & \ddots & & \vdots \\ \vdots & \ddots & \ddots & \ddots & \ddots & \vdots \\ \vdots & & \ddots & -1 & 1 & 0 \\ 0 & \cdots & \cdots & 0 & -1 & 1 \end{bmatrix} \boldsymbol{b} \succeq v_{\text{min}} \begin{bmatrix} \Delta T_{\text{out}} \\ \vdots \\ \vdots \\ \vdots \\ \Delta T_{\text{out}} \end{bmatrix}$$

3) with

$$\boldsymbol{a} \preceq \boldsymbol{b} \preceq (v_{\text{min}}/v_{\text{max}})\boldsymbol{a} + (1 - v_{\text{min}}/v_{\text{max}})x_{\text{ex}}[1, \ldots, 1]^T$$

where $\boldsymbol{a} = [a_1^0, \ldots, a_N^0]^T$ and $\boldsymbol{b} = [b_1, \ldots, b_N]^T$. Note that the right-hand side of part 2 can be changed to $[\Delta T_1, \ldots, \Delta T_N]^T$ to account for time-varying metering conditions. The advantage of this formulation is that any linear objective function may be given and optimized. In the present case, the objective function is the arrival time of the last aircraft in the stream. Conditions for shock monotonicity (9) derived earlier are still valid locally for any solution derived with the preceding linear program.

Sector Overload Predictions

When the analysis of the preceding section is used, the dynamic capacity of a sector can be predicted. Consider the worst-case

scenario: An inbound stream of aircraft, with each aircraft at v_{max} speed, is separated in time by ΔT_{in}, such that the second condition in Eq. (9) is violated. For the example shown in Fig. 6, such a stream would cause the traffic congestion to propagate from sector 34 to sector 33. Let l be the arc length distance of the portion of the arrival airway contained in sector 34 in Fig. 6. Assume that the sector is initially empty. When Eqs. (8) are used, the maximum number N_{limit} of aircraft that can be stacked along the length l of the airway in the sector until this airway is saturated can be computed. These aircraft are labeled as "metered stream" in Fig. 6. Figure 6 shows that approximately one-half of l is occupied by the metered stream at the time considered, and so the number of metered aircraft is approximately $N_{limit}/2$. When the number of metered aircraft reaches N_{limit} after a time T_{limit}, the rest of the aircraft have to be slowed down upstream in sector 33. N_{limit} and T_{limit} are given by

$$N_{limit} = \frac{l(v_{max} - v_{min})}{v_{max} v_{min}(\Delta T_{out} - \Delta T_{in})} \tag{10}$$

$$T_{limit} = \frac{l}{v_{max} v_{min}} \frac{v_{max}\Delta T_{in} - v_{min}\Delta T_{out}}{\Delta T_{out} - \Delta T_{in}} \tag{11}$$

The foregoing results have been obtained by accounting for how long it takes for congestion to grow by a length of l and how many aircraft are needed in the process. In mathematical terms, the result is obtained by solving for N_{limit} and T_{limit} in the following equations: $x_{N_{limit}}^{switch} - x_1^{switch} = l$ and $t_{N_{limit}}^{switch} - t_1^{switch} = T_{limit}$, where the switching times and locations are related by Eq. (8).

If aircraft are initially present in the sector, these two quantities can be modified by replacing l by the distance to the last aircraft in the sector. N_{limit} is referred to as dynamic capacity because it depends on inflow and outflow conditions in addition to geometric parameters.

Also note the following 1) As $v_{min} - v_{max} \to 0$, $N_{limit} \to 0$ because aircraft cannot be slowed down to meet the metering constraints; this means that if this portion of airspace is already congested, no further aircraft can be handled by it. 2) As $\Delta T_{out} - \Delta T_{in} \to 0$, $N_{limit} \to \infty$ and $T_{limit} \to \infty$: If the inbound flow is almost metered, little additional control is required for meeting the metering constraint at the outflow boundary. As a consequence, the number of aircraft required to saturate this airspace becomes large, and the time it takes to saturate this sector grows accordingly.

The switching curve $(x_i^{switch}, t_i^{switch})$ generated using Eq. (8), for example, in Fig. 8, can be used to compute the maximal extent of traffic congestion along the airway. The edge of the traffic congestion, called x_m, obtained at t_m, gives the worst situation obtained from the initial configuration a_i^0 of the aircraft. For the scenario in Fig. 8, the traffic congestion does not propagate more than 300 n mile upstream from the destination of the aircraft x_{ex}. Therefore, metering is not required upstream from that point. Because such information is unavailable currently to the ATC, controllers pass the metering restrictions upstream, which leads to flow inefficiency, or virtual overloads.

Validation Against ETMS Data

The mathematical models described in the preceding sections are now validated using a realistic simulation. The design of a simulator and its validation against ETMS data are also discussed in the next subsection. In the following subsection, the analytical predictions derived earlier are validated using the simulator. Finally, in the last subsection, the simulator is used for deriving conditions on the decorrelation of flow metering and conflict resolution.

Simulator Design

The simulator was designed following the observed control actions of the controller at the Oakland ARTCC. Figure 4 summarizes the model of the control actions observed at the ARTCC. The switching logic is implemented in the form of a cost function, which is also described in this section.
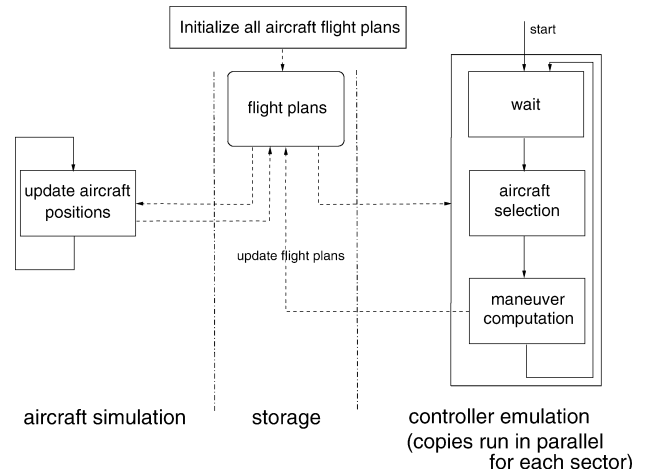

Fig. 9   Program flow of simulator.

Overall Program Flow

The overall program flow of the simulator is shown in Fig. 9. The input is a set of filed flight plans that are either user generated or taken from ETMS data. As in the real system, these flight plans are not conflict-free and usually do not satisfy metering conditions imposed on the network. Once the program is initialized, aircraft position is obtained by integrating the equations of motion (1) along the route specified via the flight plan. As time advances, conflict, as well as metering constraints, are dealt with on a sector by sector basis by predicting forward in time the actions the controller would choose to resolve conflicts and meet the metering conditions.

Key Data Structures

Given a route of flight and initial conditions, aircraft dynamic equations (1) are integrated forward to generate the aircraft trajectory. This trajectory is then implemented as a linked list of points $[x, y, z]$, with a prescribed velocity between the points, and is subsequently modified by the air traffic controller model in the program. The output for each aircraft is the updated linked list. The sectors are also implemented as sets of linked lists with data such as metering conditions (number of aircraft through a given boundary per unit time).

Air Traffic Controller Model

ATC control actions are modeled by three levels of priority:

1) Priority 1 is that there is no loss of separation (LOS). The primary requirement for ATC is to ensure that any aircraft pair is always separated by more than $\frac{3}{5}$ n mile horizontally or 1000/2000 ft vertically.[1]

2) Priority 2 is that metering conditions are met. The controller needs to ensure that the outbound traffic is adequately separated to meet the metering restrictions at the next sector (or TRACON).

3) Priority 3 is the best possible throughput. Controllers will give direct routes to aircraft if requested to minimize their flight times.

These priorities may be modeled using the following cost function J:

$$J = cost_{LOS} + cost_{BC\,breach} + cost_{delay}$$
$$+ cost_{aircraft\,actuation} + cost_{maneuver} + cost_{min\,dist} \tag{12}$$

Each term of the cost is a weighted function:

$$J = \sum_{i=1}^{N} \frac{n_{LOS}^i \cdot w_{LOS}}{\Delta T_{LOS}^i} + \sum_{i=2}^{N} \left(T_{breach}^i\right)^2 \cdot w_{breach}$$
$$+ \sum_{i=1}^{N} \left(TOA_{pred}^i - TOA_{real}^i\right) \cdot w_{delay}$$
$$+ N_{moved} \cdot w_{single\,move} + \sum_{i=1}^{N} J_{maneuver}^i + \sum_{i=1}^{N} f\left(d_{min}^i\right) \cdot w_{dist}$$

where w is the weight.

1) The LOS cost n^i_{LOS} is the number of predicted losses of separation involving aircraft i in the current sector with its current flight plan. $\Delta T^i_{\mathrm{LOS}}$ is the time until the first LOS for aircraft i.

2) The boundary condition (BC) breach cost T^i_{breach} is the time by which an aircraft violates the ΔT time separation constraint from its predecessor (set to zero if the two aircraft are separated by more than ΔT).

3) The delay cost, $\mathrm{TOA}^i_{\mathrm{pred}} - \mathrm{TOA}^i_{\mathrm{real}}$, accounts for the difference between predicted and actual time of arrival (TOA) at the last waypoint of the flight. Positive delays are penalized; earlier arrivals are favored because they reduce the flight times of aircraft. $\mathrm{TOA}^i_{\mathrm{pred}}$ and $\mathrm{TOA}^i_{\mathrm{real}}$ are computed by integration of the flight plans for each aircraft, respectively, using the original and the amended flight plans.

4) The aircraft deviation cost N_{moved} values accounts for the number of flight plan modifications chosen in the current solution. Large N_{moved} are penalized because the solution chosen by the ATC is often the simplest.

5) The maneuver cost J^i_{maneuver} accounts for the cost of the maneuver selected for aircraft i. Not all maneuvers are of equal preference, and, therefore, they have different costs. It is as easy for a controller to prescribe a 10% speed change, a VFS, or a shortcut. A holding pattern is the least preferred option because it requires constant monitoring of the aircraft. This is reflected in the choice of weight: $J^i_{\mathrm{speed\ change}} \sim J^i_{\mathrm{shortcut}} \sim J^i_{\mathrm{VFS}} \leq J^i_{\mathrm{holding\ pattern}}$. The ratio $J^i_{\mathrm{holding\ pattern}}/J^i_{\mathrm{speed\ change}}$ is of the order of 10.

6) The minimal distance cost $f(d^i_{\mathrm{min}})$ penalizes aircraft distributions in which aircraft are closely spaced (but do not lose separation) against more sparse distributions. Here, $\mathrm{dist}_{\mathrm{max}} = 7$ n mile:

$$f\left(d^i_{\mathrm{min}}\right) = \frac{1}{d^i_{\mathrm{min}}} \cdot w_{\mathrm{dist}} \qquad \text{if} \qquad d^i_{\mathrm{min}} < \mathrm{dist}_{\mathrm{max}}$$

$$f\left(d^i_{\mathrm{min}}\right) = 0 \qquad\qquad\qquad \text{otherwise}$$

To reflect the three levels of priority of the air traffic controller stated earlier, the weights shown in the cost function J are $w_{\mathrm{LOS}} \sim 10^{300} \gg w_{\mathrm{breach}} \sim 10^4 \gg$ other weights ~ 10. Thus, a computation for minimizing J first deals with losses of separation, then metering conditions, and finally optimization of the flow. The characteristics of the cost function for a two-aircraft scenario are illustrated in Fig. 10. At the top of Fig. 10, cost values for all possible maneuver combinations in a two-aircraft intersection scenario are shown, where the eight maneuvers of Fig. 4 are enabled (thus, generating $8^2 = 64$ possible values of J). Four out of 64 examples are extracted and illustrated in the bottom part of Fig. 10. At point a in Fig. 10, both aircraft A and B maintain same speed. At point b, aircraft A takes a shortcut whereas aircraft B maintains the maximum speed. At point c, aircraft A makes a VFS at low speed. At point d, aircraft A is trying to take a shortcut, which is not possible in the current flight plan. Because the move is infeasible, the maximum cost is associated to it. The controller model would choose solution b because it has the lowest cost. The cost J has been truncated at 5×10^3 for readability.

To reduce the computational time, the maximum number of aircraft controlled by the controller model in each time iteration is limited to N_{choice}. N_{choice} is chosen according to real time restrictions and computational power. If a decision needs to be made within 30 s, the value $N_{\mathrm{choice}} = 8$ is realistic. The choice of N_{choice} is a tradeoff

between running time and control quality in the simulations. It was set in the range from four to eight for the simulations. Aircraft are selected according to the following rule: Aircraft involved in LOS are selected first, then aircraft violating metering constraints are selected, and, finally, the remaining aircraft are selected until the selection list reaches N_{choice} aircraft, or until there are no more aircraft left to select. In practice, $4 \leq N_{\mathrm{choice}} \leq 8$ was found to be suitable; $N_{\mathrm{choice}} = 8$ results in more complicated maneuvers but makes the simulation run more slowly. The set of all maneuver combinations for the N_{choice} aircraft is called the maneuver set.

At each iteration of the controller action loop, an exhaustive search on the maneuver set of the chosen aircraft is run to find a set of N_{choice} maneuvers that minimizes J. The computational complexity of finding the optimal J for N_{choice} aircraft capable of n_{maneuver} possible discrete maneuvers is $\mathcal{O}[(n_{\mathrm{maneuver}})^{N_{\mathrm{choice}}}]$. This complexity can be reduced to $\mathcal{O}[(n_{\mathrm{maneuver}} - 2)^{N_{\mathrm{choice}}}]$ as follows: 1) The cost of the current maneuver has already been computed in the previous step and, thus, does not need to be recomputed. 2) Two maneuvers are mutually exclusive; therefore, only one needs to be considered. When the complexity of checking for conflicts is added, the total computational complexity of each iteration becomes

$$\mathcal{O}\left(N^2 \cdot (n_{\mathrm{maneuver}} - 2)^{N_{\mathrm{choice}}}\right)$$

where N represents the total number of aircraft in the sector. Because of both the discretization of time and the restriction of the search space to a manageable number of aircraft, the search process is not guaranteed to find the global optimum. However, it is shown in the next section that the search does provide a reasonable approximation of the controller's actions. The last parameter to adjust is the time between two successive controller activations, ΔT_{act}, the order of which is from 5 to 30 s, which is the time between successive communications of ATC with different aircraft.

Controller Model Validation Against ETMS Data

The controller model presented in the preceding section resulted from observations of air traffic controller action at the Oakland ARTCC. The modeling into a set of preferred directives has been experimentally validated for a different airspace.[21] Note, however, that even if the automaton of Fig. 4 and the cost function of the preceding section implemented in the simulator are consistent with the observations, there is no a priori guarantee that the model based on these would replicate the control actions of a human controller. For this reason, an assessment of how well the controller model describes the decision making of a human controller is needed via comparisons against recorded aircraft trajectories. Recorded ETMS data have been used as the source of actual trajectories flown in the NAS. The data extraction process that enabled conversion of ETMS data to a readable format for our simulator is described hereafter.

Data Extraction

Two types of information are provided by the ETMS data: The actual track flown by the aircraft, and the filed flight plans for each aircraft, which are amended to reflect rerouting. The track position is provided as latitude/longitude. The filed flight plan is given in terms of navigation aids, fixes, and airways, which can be looked up using a public database (URL: http://www.airnav.com). Future versions
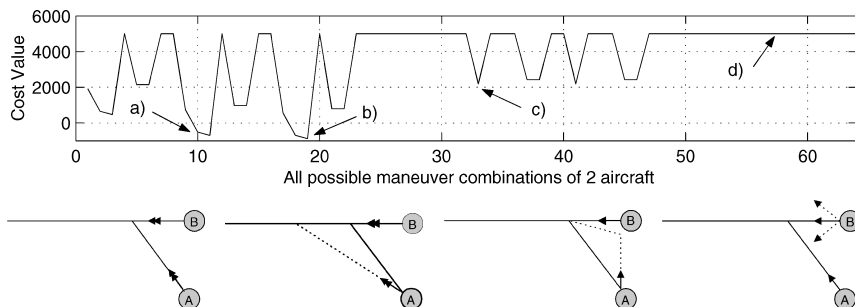
Fig. 10 Top, cost values for all possible maneuvers and bottom, maneuvers a, b, c, d labeled at top.
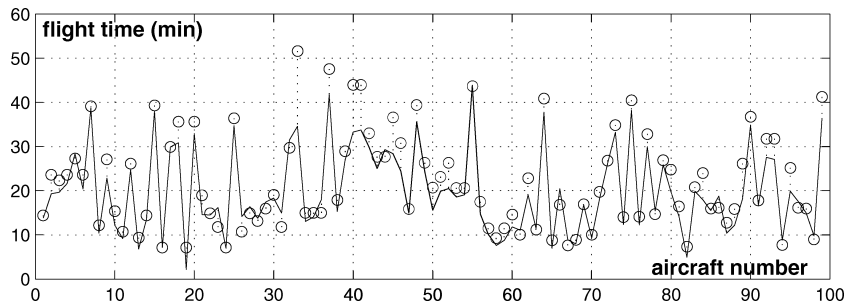
Fig. 11   Flight time comparisons for first 100 aircraft going through sector 33 in ETMS data set used.

of the simulator might use recently developed ETMS analysis tools such as those in Ref. 13. This study focuses on sector control, therefore, the traffic management unit (TMU) actions are not modeled. TMU operates at the ARTCC level (Fig. 1) and makes strategic flow scheduling decisions that go beyond the control actions of a single sector controller. Thus, the simulator needs to be validated at a scale at which TMU actions are already incorporated in the flight plans (typically one or two sectors). Because this study focuses on sectors 32, 33, 34, 15, and 13, the flight plans are truncated to be within the bounds of these sectors. The estimated TOA in the sector is set to the actual TOA as marked by the track position. The entrance location is taken to be the track position closest to the point of intersection of the flight plan and the sector boundary. The altitude assigned is the average altitude of the actual trajectory in that sector.

Validation

Comparison of flight times.   Track positions of the first 100 aircraft that flew above 33,000 ft for more than 6 min were extracted from ETMS data. Their recorded trajectories are extracted as sequences of waypoints that are used as flight plans for the simulations. Simulations were run for the following set of Mach numbers: $M \in \{0.6, 0.7, 0.8\}$ corresponding to the observations in the data for this altitude. During the simulation, the controller model is invoked every $\Delta T_{\mathrm{act}} = 10$ s. The resulting flight times are compared against actual flight times in Fig. 11. In Fig. 11, the dots are the flight times for the ETMS recorded points. The solid curve is the result of the simulations. Two main conclusions can be made. 1) The simulator is able to recreate the flow characteristics seen in ETMS data and predicts and resolves conflicts when aircraft could be separated by less than 5 n mile at the same altitude. 2) The flight time comparisons between simulated and ETMS data (Fig. 11) show a good match. The flight times provided by the simulator are usually shorter than in ETMS data because the simulator maximizes the throughput in the sector. The mean deviation was found to be 120 s for flights with an average duration of 1300 s, which amounts to a 9.2% error.

Validation of conflict resolution.   A total of 314 aircraft flying through sector 33 in a time period of 10 h was simulated. The filed flight plans were not conflict free to begin with. The simulator with the controller model modifying the trajectory every $\Delta T_{\mathrm{act}} = 20$ s is able to provide a conflict-free environment. [$\Delta T_{\mathrm{act}} = 10$ s or $\Delta T_{\mathrm{act}} = 20$ s is on the order of the maximal actuation rate of a controller. We choose $\Delta T_{\mathrm{act}} = 20$ s in this particular case because of the duration of the computation (10 h of real time simulated).] The set of speeds allowed is $M \in \{0.55, 0.75, 0.89\}$. During the simulation, trajectories of 50 aircraft were altered to resolve conflicts.

Validation of maneuver assignments.   The validation so far has shown the correlation of flow patterns generated by the simulation and those observed in reality. The next step is to validate the type of maneuver chosen by the controller model as a consequence of the minimization procedure. There were 314 flights examined in sectors 33 and 20. Different maneuvers were identified for the purpose of validation. Aircraft that followed their flight plans were assigned their actual routes of flight, and the aircraft that maneuvered to avoid conflicts were assigned their filed flight plans via a set of waypoints. The simulator was, thus, placed in the same situation as the human controller. The simulator was able to reproduce correctly 16 out of
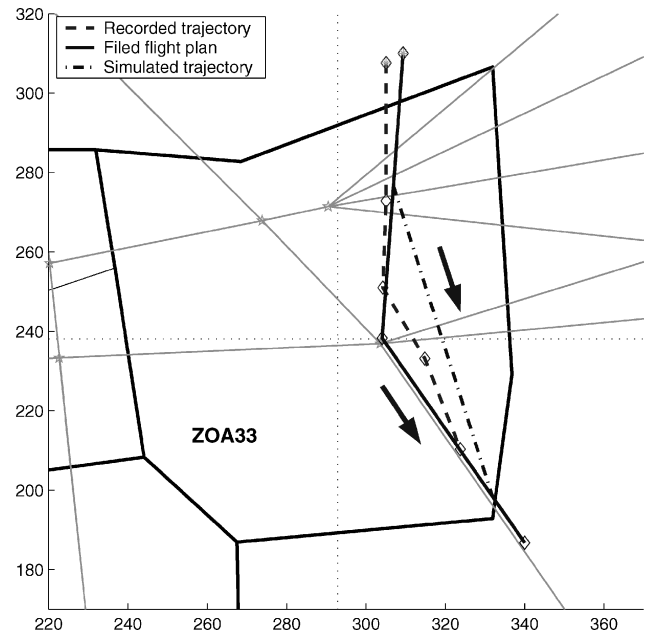

Fig. 12   Example of maneuver caused by conflict resolution, reproduced by simulator.

20 maneuvers. [Small-scale maneuvers are less likely to be executed correctly by the simulator because the probability of selecting the respective aircraft at exactly the right time is small, which explains the small discrepancy between the results. Also, even if the maneuver is executed correctly by the simulator, the resulting flight plan will look different from the ETMS data because the simulator is restricted to a single angle of deviation ($\theta = 22.5$ deg).] The simulated maneuvers, thus, appear to be reasonable and consistent with observed controller behavior. These results, thus, constitute a validation for the specific circumstances of the 20 scenarios investigated from the 314 flights considered. A more extensive simulation validation might incorporate more flights and scenarios. Also note that observations realized at the Oakland Center made such a validation sometimes impossible: It is not uncommon to ask different human controllers to solve the same problem (on paper or in a simulation) and to get two radically different answers. Thus, a full match is practically impossible. An example of good match is shown in Fig. 12. In Fig. 12, the recorded data (dashed) exhibit an actual shortcut from the filed flight plan (solid). The simulated trajectory (dashed–dotted) is a shortcut of the same type.

Validation of the Analytical Predictions

In this section, the analytical predictions are compared with simulations. An example of two backpropagating shocks, solved with an extension of the method explained earlier, is presented. Two streams, each at 10 miles in trail, are subjected to 15 miles-in-trail and 20 miles-in-trail outbound conditions. The miles-in-trail restriction for the second stream starts after all aircraft of the first stream have reached the TRACON at $t = 4300$. Speeds are
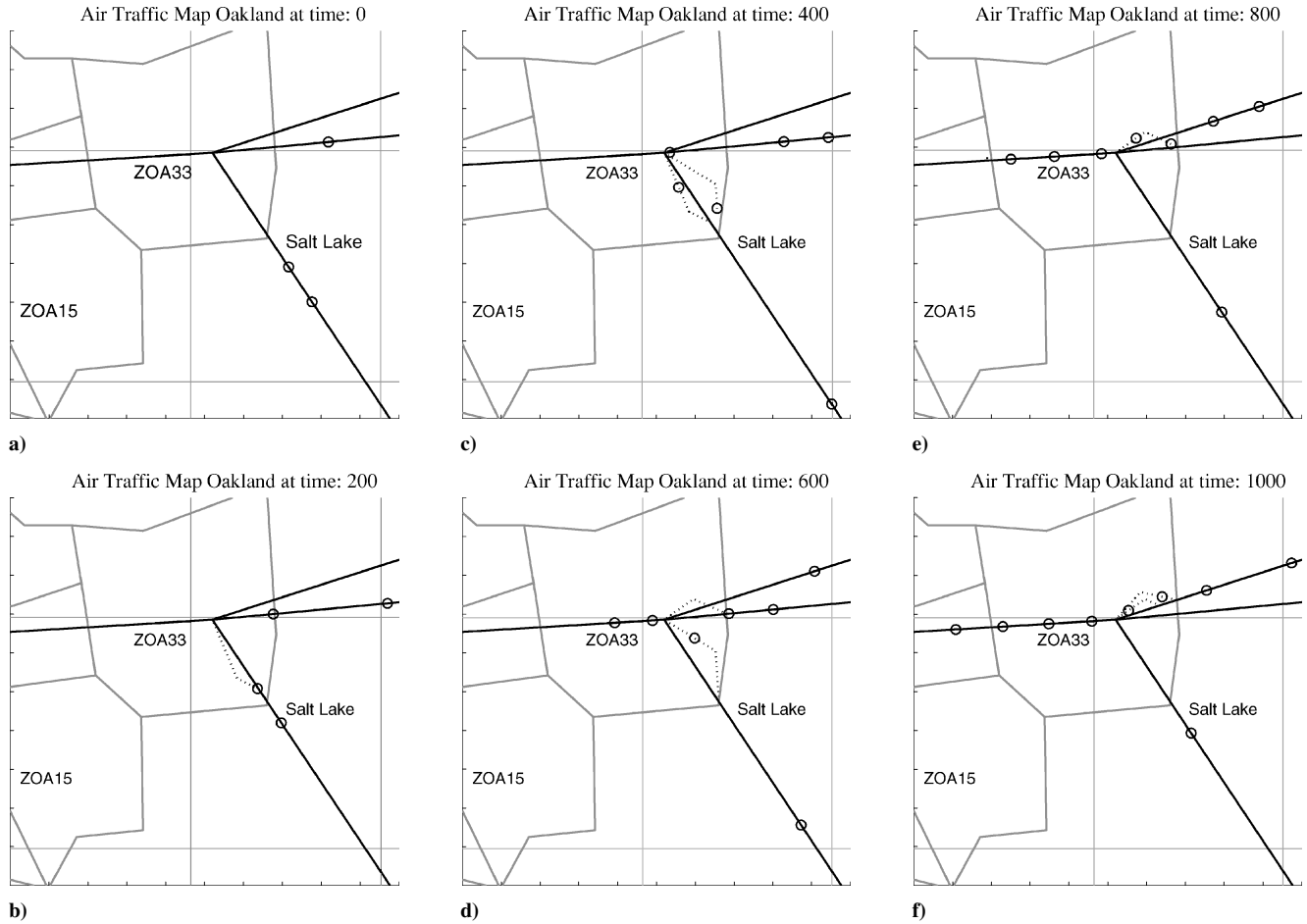
Fig. 13 Sector 33, traffic flow for merging traffic simulation of Figs. 15 and 14.
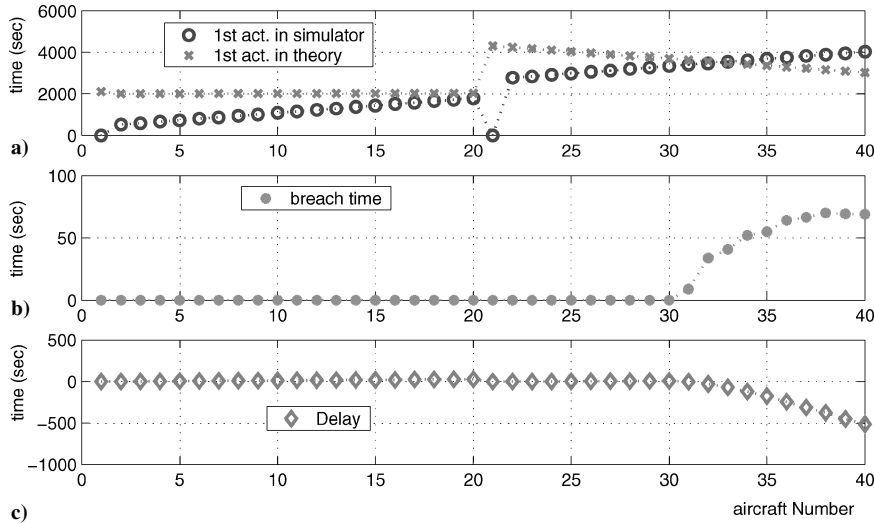

Fig. 14 First actuation times of, aircraft; breaches in metering conditions; delays of two streams of Fig. 15.

$M \in \{0.59, 0.75, 0.89\}$. The resulting aircraft flows for this analytic solution are shown in Fig. 13. In Fig. 13, the radius around the aircraft is 2.5 n mile. The solid lines represent the aircraft's flight plan. The dotted lines correspond to maneuvers assigned by the simulator. The six panels of Fig. 13 show how VFS is used by the simulator to achieve the required metering. Figure 14a shows the first actuation times of the aircraft, simulated and predicted; Fig. 14b shows breaches in metering conditions, simulated; and Fig. 14c shows delays, simulated, for the case of the two streams of Fig. 15. Figure 15 shows shocks generated by two successive streams. The first shock is steady in time. (It only propagates backward in space.) It corre-

sponds to a piling up process on a highway where all vehicles slow down at the same time. The second shock propagates backward in space and time (which is much harder to handle in practice because actuation must be performed upstream first). From Fig. 15, one can see that within the second stream, the first 12 aircraft need to be controlled within the Oakland Center, whereas the last eight need to be controlled upstream (Salt Lake Center). Because, in general, no knowledge of the required metering conditions is propagated upstream, the last eight aircraft would not be moved until they enter the Oakland Center, and no solution to this metering problem would be found without putting the aircraft on hold.
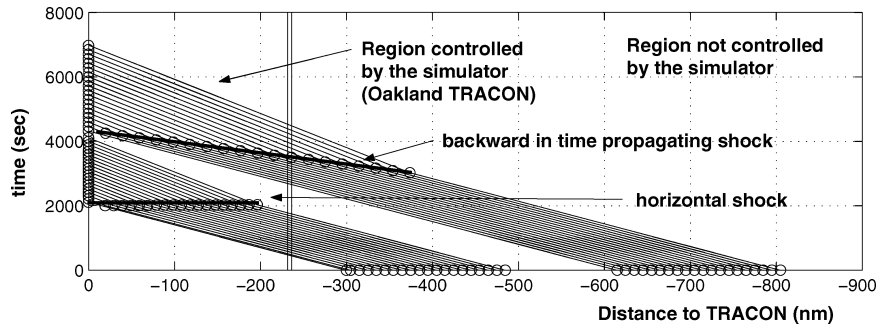
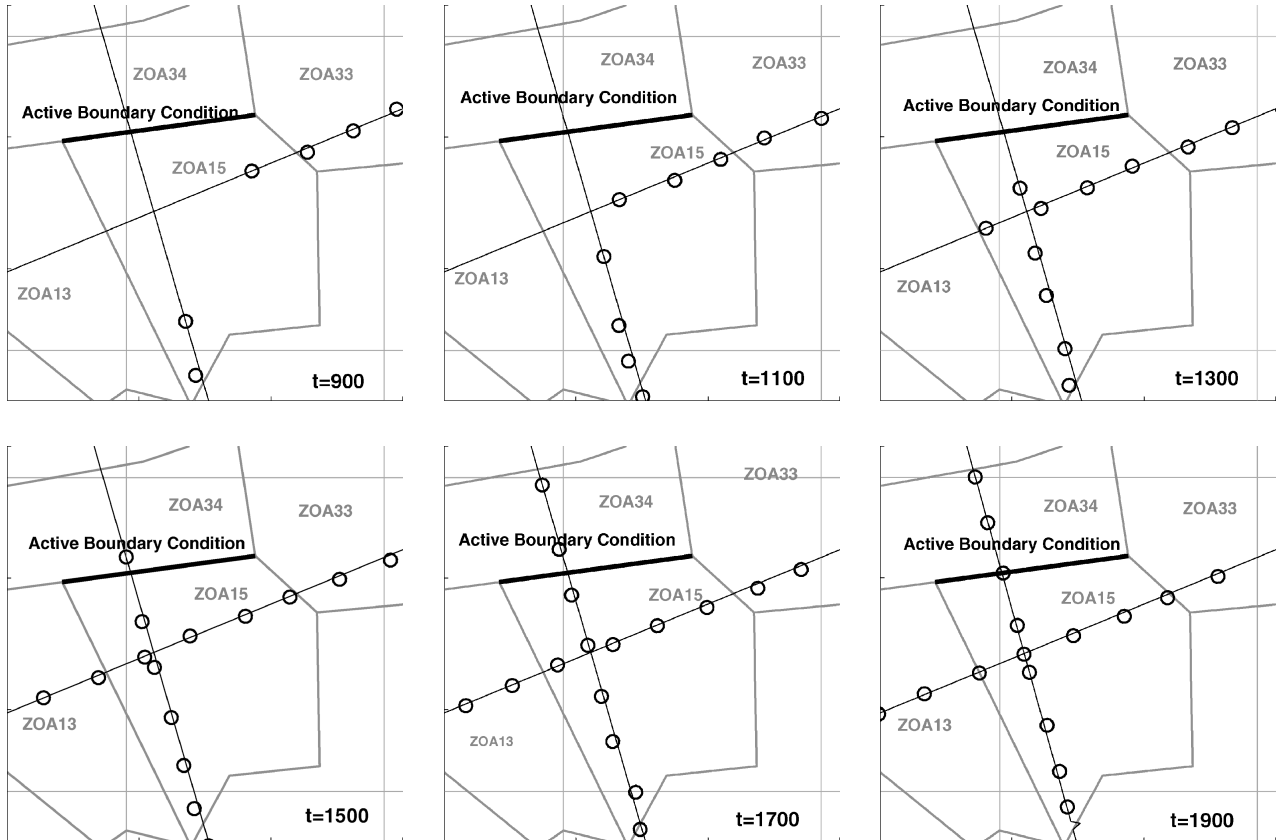Fig. 15 Shocks generated by two successive streams.

Fig. 16 Two intersecting streams, 20 miles-in-trail inbound separation.

These results are verified by simulating this flow. In Fig. 14a it can be seen that for the last eight aircraft, the first actuation time in the simulator is higher than the predicted time. The controller model is unable to control the aircraft in time because they are not in its airspace. Figure 14b shows that these aircraft are unable to meet the metering conditions by about 1 min each. This is also shown in Fig. 14c. The delays become negative; that is, the aircraft arrive in advance. This is an illustration of distributed and decentralized control: The control occurs in different sectors, and the only communication between the sectors is through the metering conditions. Obviously, the lack of centralized control (here communication and strategic TMU planning) limits efficient flow scheduling.

Decorrelation of Flow Metering and Conflict Resolution

An assumption that is often made in flow scheduling is that maneuvers for conflict avoidance do not impact metering when traffic density is low. This property of the flow is demonstrated by simulating two streams of intersecting and conflicting aircraft. Figure 16 shows two streams of aircraft intersecting at a navigation aid (Clovis, in Sector 15). Deviations (VFS) are barely visible in Fig. 16 because of their small amplitude (5 n mile). One stream is subject to metering conditions at the boundary of sectors 15 and 34 whereas

the other stream is unrestricted. The goal is to quantify the impact of the second stream on the travel times of the first stream through the sector.

There were 16 different configurations investigated by selecting combinations of the same miles-in-trail inflow restrictions for the two streams: $\Delta L_{in} \in \{15, 20, 25, 30\}$, and the following restrictions for the stream heading toward sector 34, $\Delta L_{out} \in \{15, 20, 25, 30\}$ (Fig. 16). The travel times for each stream without the presence of the other are compared with the travel time when the two streams intersect. For each configuration, 10 simulation runs were made with the initial position of the aircraft perturbed by a uniform noise of amplitude 2 n mile. This value was chosen to maintain pairwise conflicts, and to disturb the conflict resolution mechanism to have a valid statistical sample. Thus, a total of 160 runs was made for the 16 configurations. (The settings for these runs are $M \in \{0.8, 0.85, 0.89\}$; the VFS maneuver was limited to a 5-n mile deviation from the original flight plan. These settings were chosen to guarantee short flight times. The interval between controller activation was set to $\Delta T_{act} = 20$ s.) This scenario represents the situation in which each aircraft from one stream conflicts pairwise with an aircraft from the second stream. It is really a worst-case scenario because in practice aircraft might fly at different altitudes. The bound provided here is,
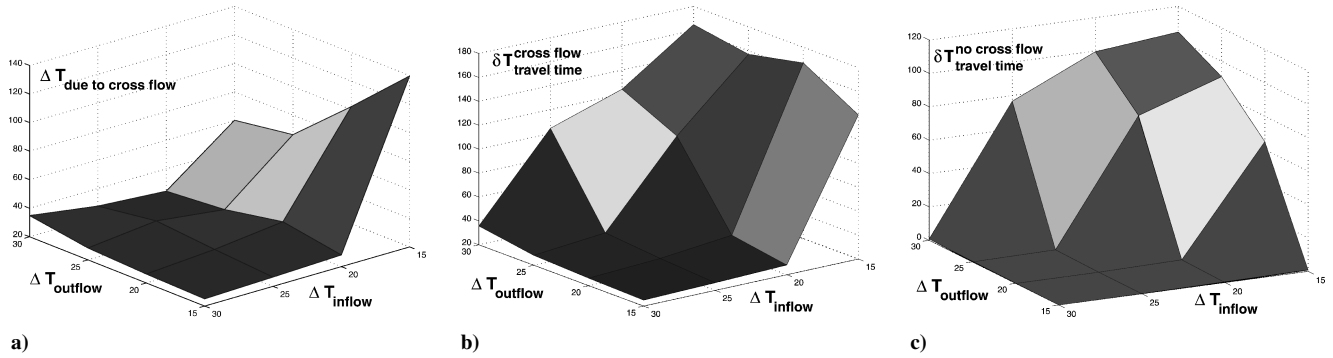
Fig. 17 Difference in delay between separate and simultaneous flow for sector 33 simulations: a) $\Delta T_{\text{due to crossflow}}$ (in seconds) averaged over 10 runs, b) $\delta T_{\text{travel time}}^{\text{crossflow}}$ (in seconds) averaged over 10 runs, and c) $\delta T_{\text{travel time}}^{\text{no crossflow}}$ (in seconds) averaged over 10 runs.

Table 1 Numerical results for decorrelation of conflict avoidance and flow metering

ΔL_{in}, n mile	ΔL_{out}, n mile	$\delta T_{\text{travel time}}^{\text{no crossflow}}$, s	$\delta T_{\text{travel time}}^{\text{crossflow}}$, s	$\Delta T_{\text{due to crossflow}}$, s
15	15	0.7	140.5	139.8
15	20	64.8	166.9	102.1
15	25	90.7	157.0	66.3
15	30	104.6	164.8	60.2
20	15	0	28.1	28.1
20	20	0.7	35.9	35.2
20	25	74.2	101.9	27.6
20	30	99.5	123.9	24.3

thus, conservative, and higher aircraft density might still be compatible in practice with metering.

For each ΔL_{in}–ΔL_{out} pair, the following quantities are computed:

$$\delta T_{\text{travel time}}^{\text{no crossflow}} = \frac{1}{N} \sum_{i=1}^{N} \left(T_{\text{aircraft } i}^{\text{no crossflow,BC}} - T_{\text{aircraft } i}^{\text{no crossflow,no BC}} \right)$$

$$\delta T_{\text{travel time}}^{\text{crossflow}} = \frac{1}{N} \sum_{i=1}^{N} \left(T_{\text{aircraft } i}^{\text{crossflow,BC}} - T_{\text{aircraft } i}^{\text{no crossflow,no BC}} \right)$$

$$\Delta T_{\text{due to crossflow}} = \delta T_{\text{travel time}}^{\text{crossflow}} - \delta T_{\text{travel time}}^{\text{no crossflow}} \qquad (13)$$

Here, $N = 20$ is the total number of aircraft with 10 aircraft in each stream. $T_{\text{aircraft } i}^{\text{no crossflow,BC}}$ represents the travel time of aircraft i in the absence of the other stream, whereas $T_{\text{aircraft } i}^{\text{crossflow,BC}}$ represents the travel time in the presence of the other stream. The results averaged over 10 runs for each case for the mean difference in travel time are shown in Fig. 17. $\Delta T_{\text{due to crossflow}}$ is shown in Fig. 17 for the complete set of (ΔL_{in}, ΔL_{out}) investigated here. The numerical values are shown in Table 1.

Even though the peak $\Delta T_{\text{due to crossflow}}$ happens for (ΔL_{in}, ΔL_{out}) = (15, 15), the maximum $\delta T_{\text{travel time}}^{\text{crossflow}}$ happens as expected for (ΔL_{in}, ΔL_{out}) = (15, 30), which is the maximal inflow/minimal outflow condition shown in Table 1. Comparing the results of Table 1 for the two values of ΔL_{in} and Fig. 17 shows the predominance of conflict resolution over BC for a high density of traffic. (See the last column in Table 1.)

The difference in delay between separate and simultaneous flow is significantly larger if the aircraft are spaced at 15 n mile when compared to streams with larger spacing, as shown in Fig. 17. Whereas the difference per aircraft is always larger than 60 s for the 15-n mile streams, it is always smaller than 60 s for streams with larger spacing. With an average flight time of 660 s over all scenarios, 60 s corresponds to an average delay of 9% in flight time. The worst-case difference (15-n mile inflow, 30-n mile outflow) is more than 21% of the overall flight time. These numbers are significant, especially when considering the possibility of multiple intersecting streams.

Note that in Fig. 17a one would intuitively expect the largest difference in delay (crossflow vs no crossflow) to happen for (ΔL_{in}, ΔL_{out}) = (15, 30), which is difficult to achieve. In fact, this maximum occurs at (ΔL_{in}, ΔL_{out}) = (15, 15). This can be explained by looking at Figs. 17b and 17c. In the absence of the second flow,

the delay accumulated due to the metering conditions is maximal for (ΔL_{in}, ΔL_{out}) = (15, 30) as expected. In the presence of the second flow, a maximum appears at (ΔL_{in}, ΔL_{out}) = (15, 15), because $\delta T_{\text{travel time}}^{\text{no crossflow}}|_{(\Delta L_{\text{in}}, \Delta L_{\text{out}}) = (15,15)} = 0$. Thus, these results are consistent. The flows in Fig. 16 represent an extreme example and are only useful for validating the performance of the underlying metering and conflict resolution algorithms.

Currently, TMU does not take the influence of conflict resolution into account when making decisions, because local conflict resolution maneuvers are not expected to increase overall flight times significantly. In some cases this assumption is untrue. Therefore, it leads to inaccuracies in the predictions of sector occupancy. Sector occupancy is defined as the number of aircraft in a sector in 15-min interval bins. Examples have been presented to show that the influence of conflict resolution maneuvers increases with higher traffic density. This requires information feedback from sector to sector such that separation and metering constraints are met.

Conclusions

A control theoretical model of sector-based traffic flow using hybrid automata theory was derived, based on observations realized at the Oakland ARTCC. A subset of this model was used for generating Lagrangian analytic predictions of the traffic flow such as dynamic sector capacity and the extent of traffic congestion. The definition of a dynamic capacity of a sector of airspace enabled quantification of the speed of propagation of congestion as a function of dynamic variables of the system, such as inbound flow and outbound restrictions, in addition to static geometric parameters such as the size of the sector. These results were linked to Eulerian models of the NAS. Applying these results enabled the derivation of conditions under which the airspace cannot be treated at the level of single sector, rather, a centralized control (communication and strategic TMU planning) would be required.

These predictions were verified against data generated by a validated simulation tool. The simulation tool consists of a model of human sector controller action on traffic, implemented in the form of a cost function for the different sectors of the airspace in consideration. This cost function was based on observations realized at the Oakland ARTCC as well, which have been validated using ETMS data. Another application of the simulation tool was demonstrated: Flow conditions under which metering can be decorrelated from conflict resolution were established.

Overall, the results of the present study suggest that the congestion speed can be correlated to dynamic variables of the system available to air traffic controllers, and conditions under which centralized action is required to operate the system efficiently can be identified. Finally, there exists a threshold density of aircraft above which conflict resolution cannot be neglected when metering the flow and preventing the extension of congestion.

Acknowledgments

References

[1]Nolan, M. S., *Fundamentals of Air Traffic Control*, 3rd ed., Brooks/Cole, Pacific Grove, CA, 1999, pp. 130–165.

[2]Perry, T. S., "In Search of the Future of Air Traffic Control," *IEEE Spectrum*, Vol. 34, No. 8, 1997, pp. 18–35.

[3]Jackson, J., and Green, S., "Control Applications and Challenges in Air Traffic Management," *Proceedings of the 1998 American Control Conference*, 1998, pp. 1772–1788.

[4]Kahne, S., and Frolow, I., "Air Traffic Management: Evolution with Technology," *IEEE Control Systems Magazine*, Vol. 16, No. 4, 1996, pp. 12–21.

[5]Gazit, R. Y., "Aircraft Surveillance and Collision Avoidance Using GPS," Ph.D. Dissertation, Dept. of Aeronautics and Astronautics, Stanford Univ., Stanford, CA, Sept. 1996.

[6]Pujet, N., and Feron, E., "Flight Plan Optimization in Flexible Air Traffic Environments," AIAA Paper 1996-3765, Aug. 1996.

[7]Plaettner-Hochwarth, J., Zhao, Y., and Robinson, J., "A Modularized Approach For Comprehensive Air Traffic System Simulation," AIAA Paper 2000-4478, Aug. 2000.

[8]Erzberger, H., Davis, T. J., and Green, S.,"Design of Center-TRACON Automation System," *Proceedings of the AGARD Guidance and Control Panel 56th Symposium on Machine Intelligence in Air Traffic Management*, AGARD, CP-538, 1993, pp. 11.1–11.12.

[9]Odoni, A., Bowman, J., Delahaye, D., Deyst, J., Feron, E., Hansman, J., Khan, K., Kuchar, J., Pujet, N., and Simpson, R., "Existing and Required Modeling Capabilities for Evaluating ATM Systems and Concepts," Dept. of Aeronautics and Astronautics, Massachusetts Inst. of Technology, Tech. Rept. NAG2-997, Cambridge, MA, March 1997.

[10]Kuchar, J., and Yang, L., "A Review of Conflict Detection and Resolution Modeling Methods," *IEEE Transactions on Intelligent Transportation Systems*, Vol. 1, No. 4, 2000, pp. 179–189.

[11]Bilimoria, K., Sridhar, B., Chatterji, G., Sheth, K., and Grabbe, S., "FACET: Future ATM Concepts Evaluation Tool," *Air Traffic Control Quarterly*, Vol. 9, No. 1, 2001, pp. 1–20.

[12]Bilimoria, K., and Lee, H., "Properties of Air Traffic Conflicts for Free and Structured Routing," AIAA Paper 2001-4051, Aug. 2001.

[13]Lin, J. C., and Gifford, D. K., "Visual Flight: The Air Traffic Control Data Analysis System," Computer Science and Artificial Intelligence Lab., Massachusetts Inst. of Technology, Tech. Rept., Cambridge, MA, May 2002.

[14]Dugail, D., Feron, E., and Bilimoria, K., "Conflict-Free Conformance to En-Route Flow-Rate Constraints," AIAA Paper 2001-4296, Aug. 2002.

[15]Mishra, P., and Pappas, G., "Flying Hot Potatoes," *Proceedings of the 2002 American Control Conference*, 2002, pp. 754–759.

[16]Innocenti, M., and Pollini, L., "Spatial Trajectory Generation for Conflict Avoidance in Air Traffic Management," AIAA Paper 2000-4070, Aug. 2000.

[17]Mao, Z., Feron, E., and Bilimoria, K., "Stability of Intersecting Aircraft Flows Under Decentralized Conflict Avoidance Rules," AIAA Paper 2000-4271, Aug. 2000.

[18]Krozel, J., Peters, M., and Bilimoria, K., "A Decentralized Control Strategy For Distributed Air/Ground Traffic Separation," AIAA Paper 2000-4062, Aug. 2000.

[19]Menon, P. K., Sweriduk, G. D., and Bilimoria, K., "New Approach for Modeling, Analysis, and Control of Air Traffic Flow," *Journal of Guidance, Control, and Dynamics*, Vol. 27, No. 5, 2004, pp. 737–744.

[20]Menon, P. K., Sweriduk G. D., Lam, T., Cheng, V. H. L., and Bilimoria, K., "Air Traffic Flow Modeling, Analysis and Control," AIAA Paper 2003-5712, Aug. 2003.

[21]Histon, J., and Hansman, R. J., "The Impact of Structure on Cognitive Complexity in Air Traffic Control," Dept. of Aeronautics and Astronautics, Massachusetts Inst. of Technology, International Center for Air Transportation, Tech. Rept. ICAT-2002-4, Cambridge, MA, June 2002.

[22]Bertsimas, D., and Stock Patterson, S., "The Air Traffic Flow Management Problem with Enroute Capacities," *Operations Research*, Vol. 46, No. 3, 1998, pp. 406–422.

[23]Bayen, A. M., and Tomlin, C. J., "Real-Time Discrete Control Law Synthesis for Hybrid Systems Using MILP: Applications to Congested Airspaces," *Proceedings of the 2003 American Control Conference*, 2003.

[24]Jeppesen Sanderson, Inc., "High Altitude Enroute Charts," URL: http://www.jeppesen.com.

[25]Dugail, D., Mao, Z.-H., and Feron, E., "Stability of Intersecting Aircraft Flows Under Centralized and Decentralized Conflict Avoidance Rules," AIAA Paper 2001-4296, Aug. 2001.

[26]Pallottino, L., Bicchi, A., and Feron, E., "Mixed Integer Programming for Aircraft Conflict Resolution," AIAA Paper 2001-4295, Aug. 2001.

[27]Bilimoria, K., "A Geometric Optimization Approach to Aircraft Conflict Resolution," AIAA Paper 2000-4265, Aug. 2000.

[28]Nilim, A., El-Ghaoui, L., Duong, V., and Hansen, M., "Trajectory-Based Air Traffic Management (TB-ATM) Under Weather Uncertainty," Proceedings of the 4rd USA/Europe Air Traffic Management R&D Seminar, Dec. 2001.

[29]Bayen, A. M., Grieder, P., Sipma, H., Meyer, G., and Tomlin, C. J., "Delay Predictive Models of the National Airspace System Using Hybrid Control Theory," *Proceedings of the 2002 American Control Conference*, 2002.

[30]Bayen, A. M., Grieder, P., and Tomlin, C. J., "A Control Theoretic Predictive Model for Sector-Based Air Traffic Flow," AIAA Paper 2002-5011, Aug. 2002.

[31]Newell, G. F., "A Simplified Theory of Kinematic Waves in Highway Traffic, Part I: General Theory," *Transportation Research*, Vol. 27, No. 4, 1993, pp. 281–287.